Journal of Alloys and Compounds 514 (2012) 103–108

Contents lists available at SciVerse ScienceDirect

Journal of Alloys and Compounds

journal homepage: www.elsevier.com/locate/jallcom

Studies of the effects of $TiCl_3$ in $LiBH_4/CaH_2/TiCl_3$ reversible hydrogen storage system

Dongan Liu[a,b], Jun Yang[a,*], Jun Ni[b], Andy Drews[a]

[a] Ford Motor Company, Research and Advanced Engineering, MD 1170/RIC, Dearborn, MI 48121, USA
[b] Department of Mechanical Engineering, University of Michigan, 1023 H. H. Dow Building 2350 Hayward Street, Ann Arbor, MI 48109-2125, USA

ARTICLE INFO

Article history:
Received 13 September 2011
Received in revised form 28 October 2011
Accepted 2 November 2011
Available online 9 November 2011

Keywords:
$LiBH_4$
$TiCl_3$
Solid-solution
Molten-solution
Reversible hydrogen storage

ABSTRACT

In the present study, the effects of $TiCl_3$ on desorption kinetics, absorption/desorption reversibility, and related phase transformation processes in $LiBH_4/CaH_2/TiCl_3$ hydrogen storage system was studied systematically by varying its concentration (x = 0, 0.05, 0.15 and 0.25). The results show that LiCl forms during ball milling of $6LiBH_4/CaH_2/xTiCl_3$ and that as temperature increases, o-$LiBH_4$ transforms into h-$LiBH_4$, into which LiCl incorporates, forming solid solution of $LiBH_4$·LiCl, which melts above 280 °C. Molten $LiBH_4$·LiCl is more viscous than molten $LiBH_4$, preventing the clustering of $LiBH_4$ and the accompanied agglomeration of CaH_2, and thus preserving the nano-sized phase arrangement formed during ball milling. Above 350 °C, the molten solution $LiBH_4$·LiCl further reacts with CaH_2, precipitating LiCl. The main hydrogen desorption reaction is between molten $LiBH_4$·LiCl and CaH_2 and *not* between molten $LiBH_4$ and CaH_2. This alters the hydrogen reaction thermodynamics and lowers the hydrogen desorption temperature. In addition, the solid–liquid nano-sized phase arrangement in the nano-composites improves the hydrogen reaction kinetics. The reversible incorporation/precipitation of LiCl at the hydrogen reaction temperature and during temperature cycling makes the $6LiBH_4/CaH_2/0.25TiCl_3$ nano-composite a fully reversible hydrogen storage material. These four states of LiCl in $LiBH_4/CaH_2/TiCl_3$ system, i.e. "formed-solid solution-molten solution-precipitation", are reported for the first time and the detailed study of this system is beneficial to further improve hydrogen storage property of complex hydrides.

1. Introduction

Complex metal hydrides are considered as potential solid state hydrogen storage material because of their high theoretical hydrogen storage capacity and adjustable hydrogen reaction thermodynamics [1,2]. Within this class of materials, $LiBH_4$ has received special interest due to its extremely high (18.4 wt%) theoretical gravimetric and (121 kg/m^3) volumetric hydrogen storage capacities [3,4]. Dehydriding of $LiBH_4$ accompanied by phase decomposition has been expressed as follows with 13.8 wt% hydrogen release [5,6]:

$$LiBH_4 \leftrightarrow LiH + B + \frac{3}{2}H_2. \quad (1)$$

However, enthalpy of the reaction above is about 72 kJ/mol H_2, which makes $LiBH_4$ too stable to become a viable on-board hydrogen storage material alone [7–9]. For example, heating above 400 °C, that is, above its melting point, is required to release its majority of the hydrogen from $LiBH_4$. Also, the rehydrogenation is not possible under moderate conditions, i.e. hydrogen pressures below 100 bar and temperature below 350 °C.

Therefore, for more than a decade, a number of studies have been conducted to reduce its dehydriding temperatures by mixing $LiBH_4$ with different additives to either modify hydrogen reaction thermodynamics and/or improve its hydrogen reaction kinetics. Züttel et al. [3] first reported that $LiBH_4$ releases small amount of hydrogen during the structure transformation around 100 °C and the major hydrogen desorption (13.5 wt%) starts at ca. 200 °C when SiO_2 powder is added. Vajo et al. [10] added 1/2 MgH_2 to $LiBH_4$ and obtained a destabilized, reversible hydrogen storage material with a reversible capacity of approximately 8–10 wt%. It was found that the addition of MgH_2 lowers the hydrogenation/dehydrogenation enthalpy by 25 kJ/(mol of H_2) compared with pure $LiBH_4$. Bosenberg et al. [11] performed a detailed analysis of the reaction mechanism of the reaction $2LiBH_4 + MgH_2 \leftrightarrow MgB_2 + 2LiH + 4H_2$. They pointed out that by adding suitable additives, the absorption and desorption temperatures can be considerably lowered and a significant enhancement of sorption kinetics obtained. Au and Jurgensen [12] evaluated various metals, metal hydrides and metal chlorides on the destabilization of $LiBH_4$ for reversible hydrogen storage. It was found that additives decreased hydrogen desorption temperature of $LiBH_4$ and improved its reversibility, but reduced hydrogen

* Corresponding author. Tel.: +1 313 337 9803; fax: +1 313 594 0502.
E-mail address: jyang27@ford.com (J. Yang).

0925-8388/$ – see front matter © 2011 Elsevier B.V. All rights reserved.
doi:10.1016/j.jallcom.2011.11.009

storage capacity. The best compromise can be reached by selecting appropriate additives, optimizing additive loading and using new synthesis processes other than ball milling. Lee et al. [13] studied the composite system of $xLiBH_4 + (1-x)Ca(BH_4)_2$ for several x values between 0 and 1, and found that the decomposition characteristics and hydrogen capacity of this composite vary with x, and the decomposition temperature is lower than those of pure $LiBH_4$ or $Ca(BH_4)_2$. Shi et al. [14] investigated the hydrogen storage properties of the mixed complex hydride $LiBH_4$–$NaAlH_4$ system, both with and without doping with $TiCl_3$ additive, and found that the doped system has a significantly lower hydrogen release temperature compared to the undoped system. Mosegaard et al. [15] investigated the interactions between $LiBH_4$ and SiO_2, $TiCl_3$, LiCl and Au. Their studies demonstrated that molten $LiBH_4$ has a high reactivity and it is a challenge to find a suitable stable catalyst.

Among different additives, Pinkerton and Meyer [16] reported $LiBH_4 + CaH_2$ as a high capacity reversible hydrogen storage system, via the following equation:

$$6LiBH_4 + CaH_2 \leftrightarrow 6LiH + CaB_6 + 10H_2 \quad (2)$$

This coupled system has a theoretical hydrogen capacity of 11.7 wt% and an estimated reaction enthalpy of $\Delta H = 59$ KJ/mol H_2. Other investigators [17–19] also reported that adding $TiCl_3$ additive into the $LiBH_4/CaH_2$ system is an effective way to obtain a lower dehydrogenation temperature. However, no efforts have been made to clarify the role of $TiCl_3$ in this system, which is urgently needed to further reveal the decomposition properties of complex hydrides and hasten their practical application. As a step towards this understanding, a systematic study of $LiBH_4/CaH_2/TiCl_3$ system in terms of the effects of varying the amount of $TiCl_3$ on its detailed decomposition properties and reaction sequences is performed.

In the present study, the $6LiBH_4/CaH_2/xTiCl_3$ ($x = 0$, 0.05, 0.15 and 0.25) nano-composites were prepared through high energy ball milling, and their hydrogen reaction properties were studied in terms of hydrogen reaction kinetics and reversibility, phase transformations and hydrogen reaction sequence. Scanning through wide composition ranges of $TiCl_3$ will provide a clear picture of the role of $TiCl_3$ in this composite system and also reveal the desorption properties of this system.

2. Experimental

2.1. Sample preparation

Lithium borohydride ($LiBH_4$) (95% purity, Sigma-Aldrich), calcium hydride (CaH_2) (98% purity, Alfa-Aesar) and titanium chloride ($TiCl_3$) (95% purity, Sigma-Aldrich) were used as received. All sample handling was performed in an MBraun Labmaster 130 glovebox maintained under an argon atmosphere. Mechanical milling was carried out using a Spex 8000 high energy mixer/mill for 2 g samples loaded into a milling vial containing two stainless steel balls weighing 8.4 g each. All the mixtures were ball milled for 5 h. For the $6LiBH_4/CaH_2/xTiCl_3$ system, its molar ratio is 6:1:x ($x = 0$, 0.05, 0.15 and 0.25).

2.2. Hydrogen storage properties analysis

Variable temperature hydrogen desorption kinetics were characterized using a water displacement desorption (WDD) apparatus (Fig. 1) constructed in-house where the desorbed gas amount was directly monitored as a function of temperature. For each experiment, a certain amount of sample was loaded into a stainless steel autoclave in the glove box. The sealed autoclave was mounted onto a three-port manifold connected to hydrogen purge gas as well as an outlet tube which passes through the bottom of a water-filled graduated burette. The manifold and sample were purged with hydrogen prior to each experiment. The sample was heated at a constant rate (5 °C/min) from room temperature to the final set point (up to 500 °C), and the desorbed hydrogen volume was monitored as the amount of water displaced in the burette. The amount of desorbed hydrogen was corrected for the reduced headspace pressure and thermal expansion of 1 bar hydrogen gas upon sample heating. Rehydriding was performed in the WDD at selected temperature and hydrogen pressure, and the reversibility was characterized through desorption using WDD.

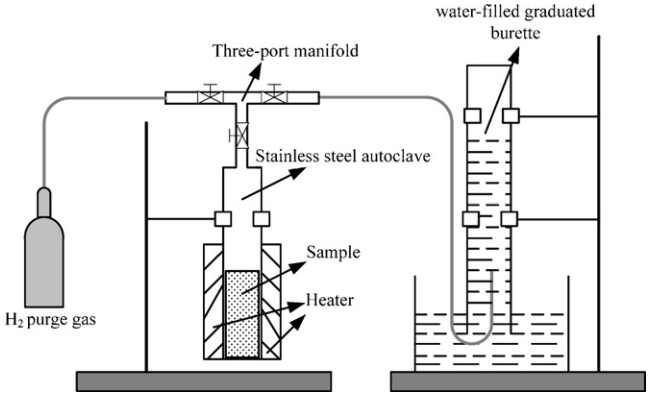

Fig. 1. Sketch of the water displacement desorption (WDD) apparatus constructed in-house.

2.3. Phase analysis

Phase transformation and chemical reactions that occurred when the sample was heated at a controlled heating rate were investigated using differential scanning calorimetry (DSC) on Setaram Sensys. The data were collected under flowing helium (20 ml/min) within a temperature range of 20–500 °C using a constant heating rate of 5 °C/min.

Phase identification and purity were characterized by Powder X-ray diffraction (PXRD). PXRD data were collected on a SCINTAG (XDS2) powder diffractometer operated at 45 kV and 40 mA with step increments of 0.02° measured during 0.5 s using Cu Kα radiation (λ = 1.5418Å). All samples were loaded in the glove box while covered with mineral oil to keep from air and maintained under a N_2 atmosphere during data collection. High-temperature X-ray diffraction data were collected using a Bueler HDK 2.4 furnace chamber attached to a Scintag X1 diffractometer, an Intel CPS 120 position sensitive detector and collimated Cu Kα radiation. Data were collected under an atmosphere of flowing purified nitrogen (200 sccm) while the temperature was ramped at a constant rate of 2 °C/min from 40 °C to 300 °C with an interval of 40 °C. At each step, the sample was held constantly for 15 min to collect data. The phase identification above 300 °C was obtained using PXRD after desorbing the nano-composite at the selected temperatures until no further hydrogen was released and then the sample was cooled to room temperature rapidly by quenching into water.

3. Results

3.1. Hydrogen desorption kinetics

In this study, samples $6LiBH_4/CaH_2/xTiCl_3$ were ball milled for 5 h to produce nano-composites. Fig. 2 shows the kinetic desorption data of each nano-composite of $6LiBH_4/CaH_2/xTiCl_3$ system with a ratio 6:1:x ($x = 0.00$, 0.05, 0.15 and 0.25). From Fig. 2, all the nano-composites present at least two desorption steps: one smaller desorption step below 400 °C and the second main desorption step between 400 °C and 500 °C. It can be seen that the nano-composite without adding $TiCl_3$ shows the worst dehydrogenation kinetics and adding 0.05 $TiCl_3$ does not improve much due to the small amount. Above around 280 °C (melting point of $LiBH_4$ (left arrow)), adding 0.15 and 0.25 $TiCl_3$ improve the dehydrogenation kinetics significantly. Further more, above around 385 °C (right arrow), the nano-composite adding 0.25 $TiCl_3$ shows the best dehydrogenation kinetics with a capacity of about 9 wt%.

The phase transformation and hydrogen desorption through chemical reactions of the post-milled nano-composites of $6LiBH_4/CaH_2/xTiCl_3$ were also analyzed by differential scanning calorimetry (DSC) as shown in Fig. 3. In each curve, three distinct endothermic peaks are apparent: the 1st and 2nd peaks, observed around 110 °C and 280 °C, correspond to the polymorphic phase transition of $LiBH_4$ from orthorhombic (o-$LiBH_4$) to hexagonal (h-$LiBH_4$) structure and the melting of $LiBH_4$ respectively. The 3rd peak corresponds to the main hydrogen desorption of the nano-composite between 385 °C and 500 °C, which is consistent with the temperature range from the kinetic desorption data (Fig. 2). Adding

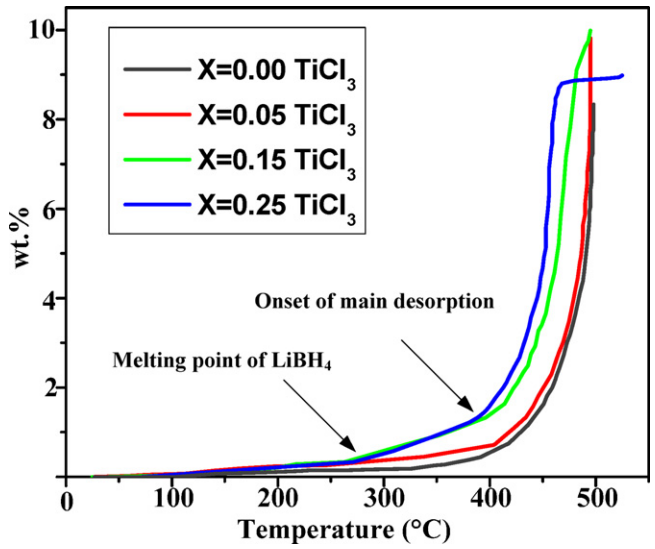

Fig. 2. Kinetic desorption data to 1 bar H_2 for $6LiBH_4/CaH_2/xTiCl_3$ (x = 0.00, 0.05, 0.15 and 0.25) nano-composites as a function of temperature (heating rate 5 °C/min).

$TiCl_3$ does not significantly lower the phase transition temperature (1st peak) and the melting temperature (2nd peak) of $LiBH_4$, which agrees with Fig. 2 (below 280 °C (melting point of $LiBH_4$)). However, for the 3rd peak, which corresponds to the main hydrogen desorption phase, adding $TiCl_3$ significantly lowers the reaction temperature (decrease by around 40 °C), especially at higher concentration of $TiCl_3$, which confirms that adding $TiCl_3$ improves the hydrogen desorption kinetics of the nano-composites (Fig. 2).

3.2. Characterization of post-milled and desorbed materials

Powder X-ray diffraction (PXRD) was used to identify the phases of the post-milled and desorbed nano-composites. Fig. 4(a) shows the PXRD patterns and corresponding phase identification for the post-milled $6LiBH_4/CaH_2/xTiCl_3$ nano-composites. From Fig. 4(a), it can be seen that the post-milled nano-composite of $6LiBH_4/CaH_2$ (without adding $TiCl_3$) is a physical mixture of $LiBH_4$ and CaH_2. When $TiCl_3$ is added, peaks of LiCl begin to appear but no peaks of $TiCl_3$ are observed and the peaks of LiCl become stronger with increasing amounts of $TiCl_3$, accompanied by a loss of $LiBH_4$ peak intensity, while CaH_2 stays intact during ball milling. Taken together, these results confirm that $LiBH_4$ and $TiCl_3$ undergo a replacement reaction. It is reported that ball milling $LiBH_4$ and $TiCl_3$ could generate an intermediate compound of $Ti(BH_4)_3$ [20,21]. If we assume that $Ti(BH_4)_3$ is one of our reaction products, the total reaction during ball milling is described as:

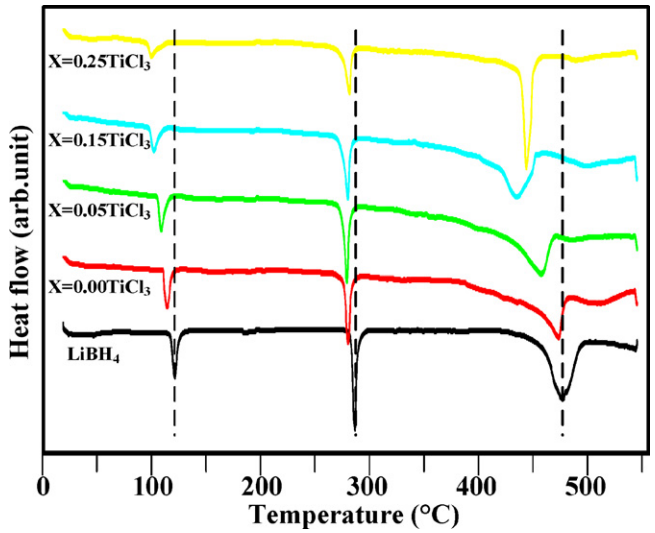

Fig. 3. DSC curves of the $6LiBH_4/CaH_2/xTiCl_3$ (x = 0.00, 0.05, 0.15 and 0.25) nano-composites (heating rate 5 °C/min).

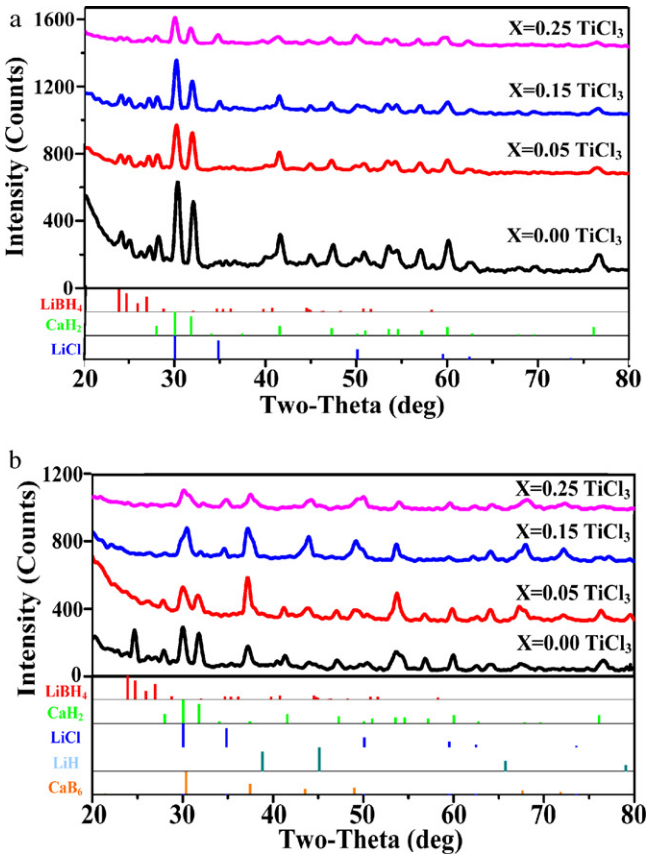

Fig. 4. (a) Room-temperature PXRD patterns and corresponding phase identification for the post-milled $6LiBH_4/CaH_2/xTiCl_3$ nano-composites. (b) R.T. PXRD patterns for $6LiBH_4/CaH_2/xTiCl_3$ nano-composites after desorption to 500 °C.

$$6LiBH_4 + CaH_2 + xTiCl_3 \rightarrow 3xLiCl + xTi(BH_4)_3 + (6-3x)LiBH_4 + CaH_2 \quad (3)$$

However, no peaks from any Ti-compound can be observed from XRD. This is possibly due to the small amount of $TiCl_3$ added, a low-temperature decomposition of $Ti(BH_4)_3$ [22] or because it remains amorphous at room temperature.

Fig. 4(b) shows the PXRD patterns for the $6LiBH_4/CaH_2/xTiCl_3$ nano-composites after desorbing at 500 °C for 10 h to 1 bar H_2 atmosphere. As shown in Fig. 4(b), for low concentrations of $TiCl_3$ (x = 0 and 0.05), un-reacted $LiBH_4$ remains. At higher concentrations, the peaks of $LiBH_4$ and CaH_2 disappear while peaks of LiCl, LiH and CaB_6 begin to emerge and grow stronger. This suggests that the post-milled nano-composite (the products side of reaction (3)) when heated to 500 °C reacts as follows:

$$3xLiCl + xTi(BH_4)_3 + (6-3x)LiBH_4 + CaH_2 \leftrightarrow (6-3x)LiH + CaB_6 + (10 + 0.5x)H_2 + 3xLiCl + xTiH_2 \quad (4)$$

3.3. Hydrogen absorption/desorption (A/D) reversibility

The hydrogen absorption/desorption reversibility was also studied using nano-composites of $6LiBH_4/CaH_2$ with and without 0.25

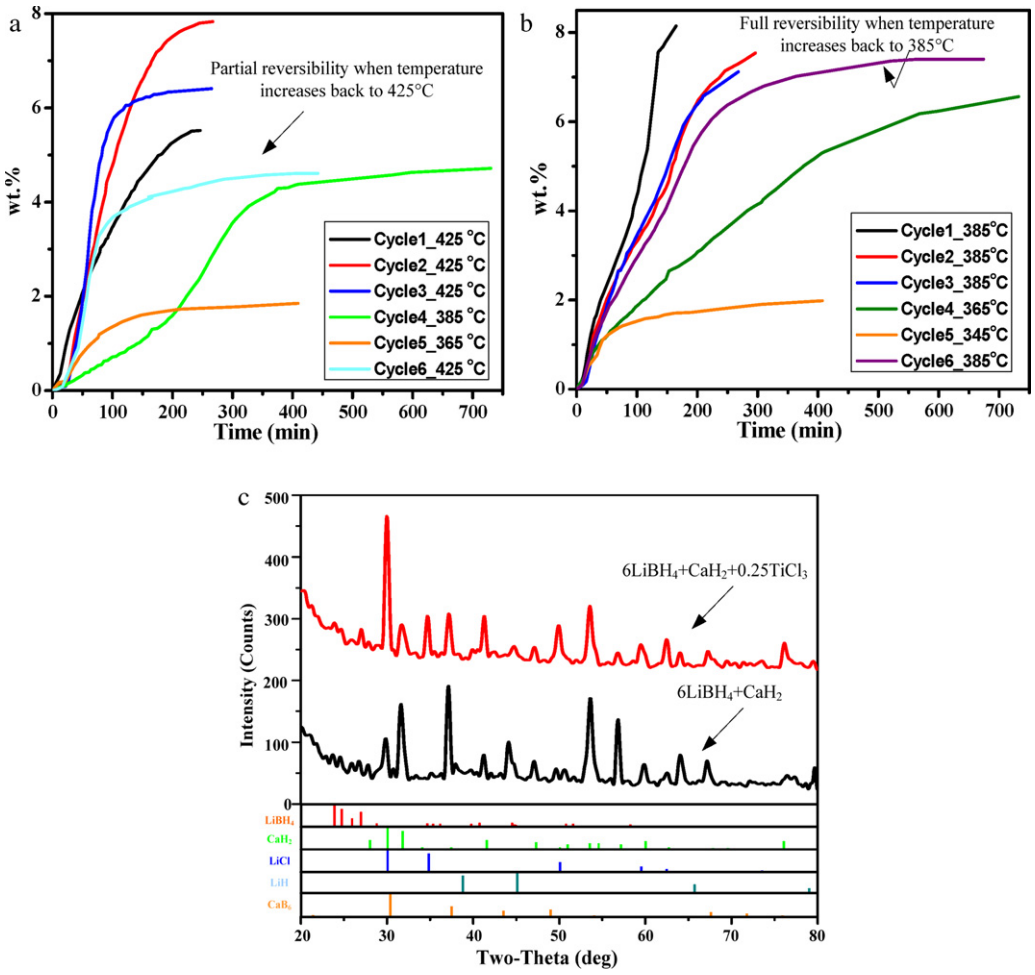

Fig. 5. (a) Hydrogen absorption/desorption reversibility of $6LiBH_4/CaH_2$ nano-composite. (b) Hydrogen absorption/desorption reversibility of $6LiBH_4/CaH_2/0.25TiCl_3$ nano-composite. (c) PXRD patterns of the two nano-composites after recharging and cooled to room temperature.

$TiCl_3$ as shown in Fig. 5(a) and (b), respectively. From Fig. 5(a), it can be seen that for the first three cycles, the nano-composite of $6LiBH_4/CaH_2$ shows a partial reversibility upon charging and desorbing at 425 °C. When the desorption temperatures are decreased to 385 °C and 365 °C respectively (4th and 5th cycles), the desorption kinetics and the amount of desorbed hydrogen decrease significantly. After the recharging and desorbing temperatures were raised back to 425 °C (6th cycle), the desorbed hydrogen capacity is only partially recovered.

On the other hand, from Fig. 5(b), it can be seen that the as-milled $6LiBH_4/CaH_2/0.25TiCl_3$ nano-composite exhibits good reversibility for the first three cycles when desorbing at 385 °C. When lowering the charging and desorbing temperatures to 365 °C and 345 °C, both the kinetics and desorption capacity are decreased, as shown in the 4th and 5th cycles, respectively. However, when the recharging and desorbing temperature is set back to 385 °C, shown as the 6th cycle, the desorbed hydrogen amount and desorption kinetics return almost to the initial level. Therefore, it can be seen that adding 0.25 $TiCl_3$ into the $6LiBH_4/CaH_2$ nano-composite can significantly improve its reversibility and also decrease the main decomposition temperature by 40 °C.

Fig. 5(c) shows the PXRD patterns of the recharged $6LiBH_4/CaH_2$ and $6LiBH_4/CaH_2/0.25TiCl_3$ nano-composites after the reversibility cycles of Fig. 5(a) and (b). As shown in Fig. 5(c), after recharging in 170 bar H_2 at 425 °C and 385 °C respectively, both $6LiBH_4/CaH_2$ and $6LiBH_4/CaH_2/0.25TiCl_3$ nano-composites returns to a mixture of primarily $LiBH_4$ and CaH_2, which confirms the reversibility of the reaction between LiH + CaB_6 and $LiBH_4$ + CaH_2 as shown in reaction (2). The main differences between these two nano-composites are: (I) the former contains more unreacted CaB_6 and LiH for the same charging period although the charging temperature is higher by 40 °C, reflecting the slow kinetics for reaction (2), leading to a deterioration in reversibility. (II) There is LiCl precipitated in the recharged nano-composite of $6LiBH_4/CaH_2/0.25TiCl_3$.

3.4. *In situ* phase transformation during desorption

In order to further understand the role played by $TiCl_3$, *in situ* PXRD of $6LiBH_4/CaH_2/0.25TiCl_3$ nano-composites were used to observe the phase changes during the hydrogen desorption process. The *in situ* XRD patterns were shown in Fig. 6. In Fig. 6(a), it can be seen that $LiBH_4$ transforms from o-$LiBH_4$ to h-$LiBH_4$ between 80 °C and 120 °C, which is consistent with the first endothermic peak (110 °C) in Fig. 3. Above 280 °C, CaB_6 and LiH begin to appear accompanied by a weakening of $LiBH_4$ and CaH_2 peaks, consistent with reaction (4). More importantly, the LiCl peaks become weaker as temperatures are increased from room temperature and disappear when the temperature exceeds 120 °C (phase transition temperature from o-$LiBH_4$ to h-$LiBH_4$), which suggests that LiCl incorporates into h-$LiBH_4$ to form a solid solution of $LiBH_4$·LiCl [15,23].

For the temperature from 300 °C to 500 °C, five nano-composites were desorbed each at a specific temperature (300, 350, 400, 450 and 500 °C) for 10 h to 1 bar H_2 pressure, respectively, and

Table 1
Four different states of LiCl during the hydrogen desorption of $6LiBH_4/CaH_2/0.25TiCl_3$ nano-composite to 500 °C.

State of LiCl	Formed	Solid solution to $LiBH_4$	Molten solution to $LiBH_4$	Precipitated
Condition	Post ball-milled	120–280 °C	280–350 °C	350–500 °C

then quenched to room temperature. Powder XRD patterns of those five quenched post-desorbed samples were used to identify phases after higher temperature hydrogen desorption, as shown in Fig. 6(b). $LiBH_4$ and CaH_2 are observed in samples quenched at 300–350 °C, although their peak intensities keep decreasing. The difference between Fig. 6(a) and (b) at 300 °C is caused by recrystallization of the molten $LiBH_4$. It is noteworthy that after desorption at 350 °C for 10 h to 1 bar H_2, the quenched sample did not show LiCl peaks, suggesting that the molten solution of $LiBH_4$·LiCl at 350 °C was frozen into a solid solution. Above 400 °C, peaks of CaB_6 and LiH become stronger along with the disappearance of $LiBH_4$ and CaH_2, which is consistent with reaction (4). Contrary to the case at 350 °C, peaks of LiCl emerge again from 400 °C to 500 °C while $LiBH_4$ disappears due to the hydrogen reaction (4). Hence, during the hydrogen desorption process, LiCl in $6LiBH_4/CaH_2/0.25TiCl_3$ nano-composite first forms solid solution ($LiBH_4$·LiCl) with $LiBH_4$, which becomes molten solution ($LiBH_4$·LiCl) as temperatures are increased to about 280 °C, and then precipitates out after $LiBH_4$ reacts with CaH_2, forming CaB_6 and LiH as summarized in Table 1.

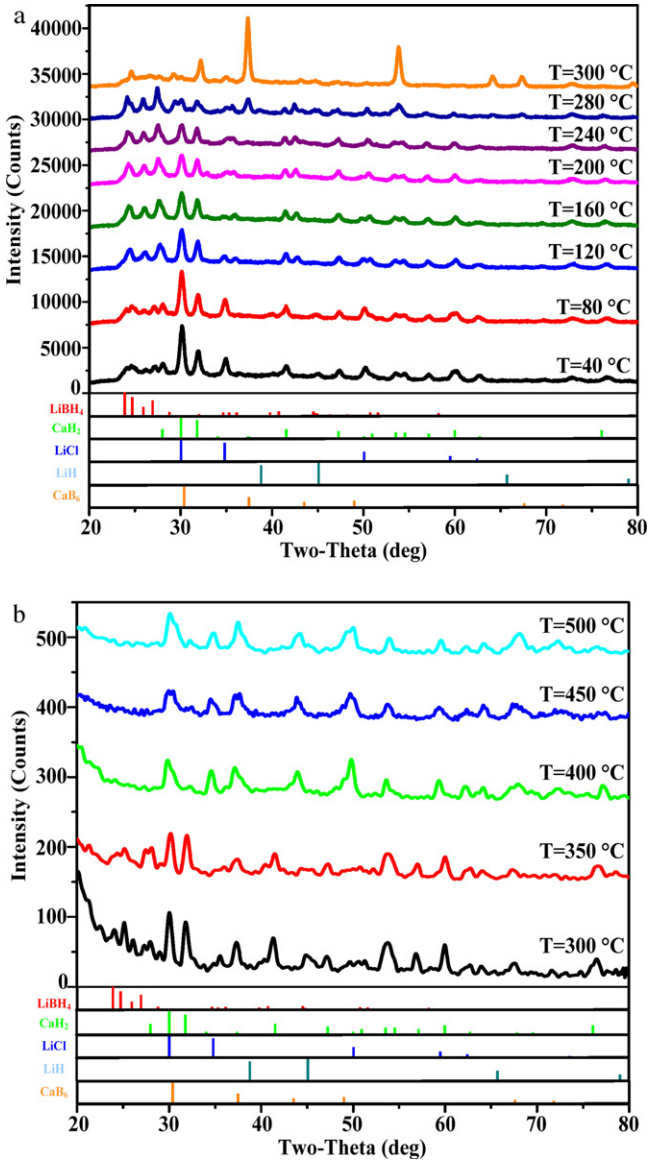

Fig. 6. (a) *In situ* PXRD patterns for $6LiBH_4/CaH_2/0.25TiCl_3$ nano-composite from 40 °C to 300 °C. (b) PXRD patterns of quenched $6LiBH_4/CaH_2/0.25TiCl_3$ nano-composites after desorbing for 10 h at 300 °C, 350 °C, 400 °C, 450 °C, and 500 °C, respectively.

4. Discussion

From Figs. 2–6, the following effects with the addition of $TiCl_3$ into $6LiBH_4/CaH_2$ nano-composite can be outlined:

(I) LiCl and $Ti(BH_4)_3$ are formed through replacement reaction (3). However, the formed $Ti(BH_4)_3$ is not stable and further decomposes to TiH_2 when temperature is increased [20]. Although, neither $Ti(BH_4)_3$ nor TiH_2 could be clearly identified from XRD measurements probably due to the small amount of $TiCl_3$ added or their amorphous nature, the existence of LiCl after ball milling must result from reaction (3) and was observed obviously from XRD, which consequently disperses TiH_2 and LiCl on the surface of particles of the nano-composites.

(II) The phase transformation of o-$LiBH_4$ to h-$LiBH_4$ and the dissolution of LiCl into h-$LiBH_4$ to form $LiBH_4$·LiCl above 120 °C, as is observed in *in situ* XRD, first as solid solution, and later as a molten solution above the melting point of 280 °C. The $LiBH_4$·LiCl remains stable up to the onset of the main hydrogen reaction between the $LiBH_4$·LiCl (liquid) and CaH_2 (solid), forming CaB_6, LiH and releasing hydrogen. When $LiBH_4$ in the molten solution is consumed, LiCl is precipitated as a solid again, as can be seen from XRD of the quenched samples (Fig. 6(b)).

The reaction between the $LiBH_4$ and $TiCl_3$ during ball milling forms LiCl through a replacement reaction (3), forming nanometer sized composite particles of $LiBH_4 + CaH_2 + LiCl + TiH_2$ (or $Ti(BH_4)_3$). As this nano-composite is heated to about 120 °C, $LiBH_4$ is transformed from orthorhombic into hexagonal structure, and LiCl subsequently incorporates into h-$LiBH_4$ to form a $LiBH_4$·LiCl solid (up to 280 °C) and molten solution (above 280 °C). The formation of the $LiBH_4$·LiCl solution changes the thermodynamics and the corresponding hydrogen desorption reaction and lowers the hydrogen desorption temperature from 425 °C ($6LiBH_4 + CaH_2$ nano-composites) to 385 °C.

(III) The much improved hydrogen absorption/desorption reversibility of the $6LiBH_4/CaH_2/0.25TiCl_3$ nano-composite compared to $6LiBH_4/CaH_2$ nano-composite result from the microstructural change due to the incorporation of LiCl into $LiBH_4$. It is experimentally observed that the incorporation of LiCl into $LiBH_4$ increases the viscosity of the molten $LiBH_4$·LiCl compared to molten $LiBH_4$ at the same temperature. A more viscous $LiBH_4$·LiCl liquid helps to prevent the excessive clustering of the molten $LiBH_4$ and the coalescence of CaH_2, preserving the nano-sized phase arrangement in the $6LiBH_4/CaH_2/0.25TiCl_3$ nano-composites which shortens the mass transfer distance during the hydrogen desorption reaction and preserves well dispersed CaB_6, LiH and LiCl nano-composites. It is also worth mentioning that the preformed TiH_2 may further prevent the grain growth of phases during the desorption process.

Similarly, upon recharging, the CaB_6 and LiH in the CaB_6/LiH/LiCl nano-composite formed during the hydrogen desorption with the nano-sized TiH_2 dotted on the grain boundaries will react to form

$LiBH_4$ and CaH_2. Once $LiBH_4$ is formed, it will combine with the precipitated LiCl, forming a molten solution of $LiBH_4$·LiCl, which is more viscous than molten $LiBH_4$, preserving the nano-sized phase arrangement in the recharging process. This well-dispersed nano-sized solid–liquid phase arrangement in the $6LiBH_4/CaH_2/0.25TiCl_3$ nano-composite is key to realizing good reversibility.

5. Conclusions

In summary, systematic studies of the phase evolution on cycling $6LiBH_4/CaH_2/xTiCl_3$ with $x = 0$, 0.05, 0.15, and 0.25 have been performed. It is found that adding 0.25 $TiCl_3$ produces reversible hydrogen absorption and desorption and a lower desorption temperature. More importantly, LiCl is formed through replacement reaction between $LiBH_4$ and $TiCl_3$ during ball milling. This LiCl then forms solid solution with $LiBH_4$ at about 120 °C when o-$LiBH_4$ transforms into h-$LiBH_4$. The $LiBH_4$·LiCl solid solution persists up to about 280 °C, where it becomes molten $LiBH_4$·LiCl, changing reactants and thus reaction thermodynamics and lowering the hydrogen desorption temperature.

On the other hand, the incorporation of LiCl into $LiBH_4$ favorably changes the viscosity of molten $LiBH_4$·LiCl, preserving the nano-sized phase arrangement formed after milling, leading to fast kinetics. Furthermore, the precipitation of LiCl from viscous $LiBH_4$·LiCl molten solution with the consumption of $LiBH_4$ upon hydrogen desorption and its re-incorporation into $LiBH_4$ upon re-hydrogenation generates a well-dispersed liquid–solid nano-sized phase arrangement at the recharging temperature, leading to a fully reversible complex hydrogen storage system at the hydrogen reaction temperature range. The full reversibility of this system is also exemplified by the fact that when the recharged ternary nano-composite is cooled to room temperature slowly, LiCl precipitates from the molten $LiBH_4$·LiCl at temperatures below 120 °C. As the temperature is increased in the next desorption, LiCl will re-incorporate into the h-$LiBH_4$ and the above cycle will continue. This more detailed study of the effect of $TiCl_3$ in $LiBH_4$-containing system will be helpful in engineering complex hydride nano-composites into practically viable hydrogen storage materials.

Acknowledgements

The authors thank Dr. Justin Purewal, Dr. Andrea Sudik and Dr. Donald Siegel for their invaluable comments and discussions.

References

[1] S.I. Orimo, Y. Nakamori, J.R. Eliseo, A. Züttel, C.M. Jensen, Chemical Reviews 107 (2007) 4111.
[2] A. Züttel, S. Rentsch, P. Fischer, P. Wenger, P. Sudan, P. Mauron, C. Emmenegger, Journal of Alloys and Compounds 356–357 (2003) 515.
[3] A. Züttel, A. Borgschulte, S.I. Orimo, Scripta Materialia 56 (2007) 823.
[4] P. Wang, X.D. Kang, Dalton Transactions 40 (2008) 5400.
[5] A. Züttel, P. Wenger, P. Sudan, P. Mauron, S.I. Orimo, Materials Science and Engineering B: Solid-State Materials for Advanced Technology 108 (2004) 9.
[6] K. Miwa, N. Ohba, S.I. Towata, Y. Nakamori, S.I. Orimo, Physical Review B - Condensed Matter and Materials Physics 69 (2004) 245120.
[7] H. Chu, Z. Xiong, G. Wu, J. Guo, T. He, P. Chen, Dalton Transactions 39 (2010) 10585.
[8] J. Yang, A. Sudik, C. Wolverton, Journal of Physical Chemistry C 111 (2007) 19134.
[9] P.A. Chater, W.I.F. David, S.R. Johnson, P.P. Edwards, P.A. Anderson, Chemical Communications (2006) 2439.
[10] J.J. Vajo, S.L. Skeith, F. Mertens, Journal of Physical Chemistry B 109 (2005) 3719.
[11] U. Bosenberg, S. Doppiu, L. Mosegaard, G. Barkhordarian, N. Eigen, A. Borgschulte, T.R. Jensen, Y. Cerenius, O. Gutfleisch, T. Klassen, M. Dornheim, R. Bormann, Acta Materialia 55 (2007) 3951.
[12] M. Au, A. Jurgensen, Journal of Physical Chemistry B 110 (2006) 7062.
[13] J.Y. Lee, D. Ravnsbæk, Y.S. Lee, Y. Kim, Y. Cerenius, J.H. Shim, T.R. Jensen, N.H. Hur, Y.W. Cho, Journal of Physical Chemistry C 113 (2009) 15080.
[14] Q. Shi, X. Yu, R. Feidenhans'l, T. Vegge, Journal of Physical Chemistry C 112 (2008) 18244.
[15] L. Mosegaard, B. Møller, J.E. Jørgensen, Y. Filinchuk, Y. Cerenius, J.C. Hanson, E. Dimasi, F. Besenbacher, T.R. Jensen, Journal of Physical Chemistry C 112 (2008) 1299.
[16] F.E. Pinkerton, M.S. Meyer, Journal of Alloys and Compounds 464 (2008) L1.
[17] J.H. Lim, J.H. Shim, Y.S. Lee, Y.W. Cho, J. Lee, Scripta Materialia 59 (2008) 1251.
[18] J.H. Lim, J.H. Shim, Y.S. Lee, J.Y. Suh, Y.W. Cho, J. Lee, International Journal of Hydrogen Energy 35 (2010) 6578.
[19] A. Ibikunle, A.J. Goudy, H. Yang, Journal of Alloys and Compounds 475 (2009) 110.
[20] Z.Z. Fang, L.P. Ma, X.D. Kang, P.J. Wang, P. Wang, H.M. Cheng, Applied Physics Letters 94 (2009) 044104.
[21] V.V. Volkov, K.G. Myakishev, Bulletin of the Academy of Sciences of the USSR Division of Chemical Science 36 (1987) 1321.
[22] M. Au, A. Jurgensen, K. Zeigler, Journal of Physical Chemistry B 110 (2006) 26482.
[23] L.M. Arnbjerg, D.B. Ravnsbæk, Y. Filinchuk, R.T. Vang, Y. Cerenius, F. Besenbacher, J.E. Jørgensen, H.J. Jakobsen, T.R. Jensen, Chemistry of Materials 21 (2009) 5772.